Composite Structures 160 (2017) 204–210

Contents lists available at ScienceDirect

Composite Structures

journal homepage: www.elsevier.com/locate/compstruct

Damage modeling for carbon fiber/epoxy filament wound composite tubes under radial compression

José Humberto S. Almeida Jr. [a,*], Marcelo L. Ribeiro [b], Volnei Tita [b], Sandro C. Amico [a]

[a] PPGE3M, Federal University of Rio Grande do Sul, Av. Bento Gonçalves, 9500, 91501-970 Porto Alegre, RS, Brazil
[b] Department of Aeronautical Engineering, São Carlos School of Engineering, University of São Paulo, Av. João Dagnone 1100, São Carlos, SP, Brazil

ARTICLE INFO

Article history:
Received 25 July 2016
Revised 11 October 2016
Accepted 15 October 2016
Available online 17 October 2016

Keywords:
Filament wound tube
Damage modeling
Finite element analysis
Radial compression
Delamination

ABSTRACT

The focus of this study is the development of a computational model with damage to predict failure of carbon fiber/epoxy filament wound composite tubes under radial compressive loading. Numerical analysis is performed via Finite Element Method (FEM) with a damage model written as a UMAT (User Material Subroutine) and linked to commercial software. The experimental analysis carried out followed ASTM D2412-11, where the specimen is parallel-loaded by two steel-based plates. Three stacking sequences have been evaluated. Both numerical and experimental results show that the presence of hoop layers at inner and outer layers plus ±75° non-geodesic layers gives maximum compressive load to the composite tube, since the reinforcement is wound closer to the loading direction. Moreover, failure modes are predominantly delaminations, which are confirmed via numerical analyses through high in-plane shear stresses levels, and via experimental analyses through stereoscopic micrographs.

1. Introduction

Cylindrical shells have numerous applications in aerospace, aeronautic and marine structures, such as in launch vehicle fuel tanks, fuselages and offshore structures. They have the ability to support high levels of axial and transverse compression loadings, where most of the structure is submitted to membrane loads, and its efficiency is derived from the lack of through-the-thickness stress gradients [1]. These structures are traditionally metallic-based, but the requirements for increasing the payload in such aeronautic and marine structures are motivating the use of polymeric composites, mainly due to their lack of corrosion and high stiffness and strength-to-weight ratios [2].

Among the composite manufacturing processes, filament winding (FW) stands out due to high precision in fiber positioning, high fiber content, good automation capability and low void content, being the most common process for manufacturing revolution and axisymmetric parts, such as pressure vessels and tubes [3]. When these structures suffer uniaxial or biaxial compression loads, the shell structure initially starts to deform stably, eventually reaching a critical point where equilibrium stops to be stable. Buckling occurs when the structure suddenly deflects unstably, losing its capacity to keep resisting the compressive loading [4].

Composite tubes may fail due to global or local buckling under compressive loadings, and they present two distinct behavior. The evolution of high radial displacements followed by global buckling and, consequently, collapse, or just a sudden collapse. The load prediction is much more difficult for composite structures than for metallic shells, beams and plates [5]. In addition, if the composite is sufficiently thick, the structure may fail due to material failure, thus avoiding buckling [6].

Damage prediction is a key aspect in the designing of composite tubular structures. Continuum Damage Mechanics (CDM) has been applied with success to model failure in composite structures. For instance, Camanho et al. [7] used CDM to predict strength and size effects in notched carbon/epoxy open-hole specimens subjected to tensile loading. Su et al. [8] developed a model using CDM for the progressive damage in open-hole specimens under compressive loading. Liu and Zheng [9] developed an energy-based stiffness degradation CDM model to predict the progressive failure of pressure vessels considering three failure modes: fiber breakage, matrix cracking and fiber/matrix interface failure.

An important parameter in the laminates is the stacking sequence, since each ply contributes to the global mechanical response. The effect of the winding sequence on the radial compressive behavior of composite tubes is significant. As shown by Melo [10], tensile strength and modulus can increase up to 20% just changing the stacking sequence in comparison to those laminates with the same ply angle throughout the laminate. The

* Corresponding author.
E-mail address: jhsajunior@globomail.com (J.H.S. Almeida Jr.).

http://dx.doi.org/10.1016/j.compstruct.2016.10.036
0263-8223/

development of a computational model to simulate damage in filament wound composite tubes allows reducing costs and time-consuming experimental tests in the development of products.

There are many reports on the literature dealing with the compressive behavior of composite tubes under axial compression [11–13]. Faria and Guedes [14] and Guedes et al. [15] performed similar experimental ring deflection tests on glass fiber/polyester pipes focusing on long-term creep behavior. However, there are only few investigations on composite tubes under radial compression. Among them, Rafiee [16] evaluated the radial compressive behavior of FW tubes by means of experimental and theoretical approaches, and Tonatto et al. [17] performed an experimental and numerical assessment of the crushing behavior of offloading hoses.

The number of damage models has increased, but failure prediction for composite structures is still a challenge, especially for tubular structures. Therefore, the present work proposes to develop a computational model to predict damage initiation and evolution of carbon fiber/epoxy composite tubes manufactured by FW and subjected to radial compressive loading, and to compare the results to those from actual experiments.

2. Damage model

Ribeiro et al. [18] developed a damage model based on CDM, which was slightly modified for the material and geometry herein used. The model considers the composite lamina under plane stress state and damage is considered uniform throughout the laminate thickness [19].

2.1. Fiber failure modeling

A unidirectional carbon/epoxy composite laminate under tensile loading in the fiber direction (σ_{11}) is assumed linear elastic with brittle fracture. The model considers that the fiber behavior is not influenced by the damage state of the matrix. The maximum stress criterion is used to identify fiber failure:

$$\frac{\sigma_{11}}{X_t} \leqslant 1 \tag{1}$$

where X_t is the strength under tension in the fiber direction.

After failure, the damage variable in the fiber direction (d_1) is set to be "1". There is no evolution in d_1, i.e. it represents the catastrophic failure of the carbon fiber. To avoid possible localization issues, degradation of properties occurs at the end of each time step through Finite Element Method (FEM) solution. In addition, no degradation is allowed during each interaction to improve convergence. This strategy is required to control the time step in order to limit the element size between a particular step (calculation of the damage) and the following step (application of the damage). Thus, a parametric step-size sensitivity analysis in the FEM should be carried out to find best results.

The fiber behavior under compressive longitudinal load is set to be linear elastic until a specified value and, after that, non-linear elastic. The linear to non-linear elastic limit (X_{C0}) is then used in Eq. (2) to represent the compressive failure, as:

$$\frac{|\sigma_{11}|}{X_{C0}} \leqslant 1 \tag{2}$$

After $|\sigma_{11}| \geqslant X_{C0}$, the non-linear elastic stress–strain behavior is simulated using a secant modulus, as shown in Eq. (3):

$$E_{11} = \frac{X_{C0}}{|\varepsilon_{11}|}(1 - h(\varepsilon_{11})) + h(\varepsilon_{11})E_{11_0} \tag{3}$$

where $h(\varepsilon_{11})$ is obtained from the fitting of stress-strain plots for 0° specimens under compressive loading, ε_{11} is the strain in the longitudinal direction and E_{11_0} is the initial elastic modulus for 0° specimens under compression loading.

2.2. Matrix failure modeling

In a unidirectional filament wound laminate, the damage process in the matrix is essentially driven by transverse loading (σ_{22}) and shear loading (σ_{12}). A non-linear behavior in the matrix is reported due to inelastic strains and matrix damage [20], being the latter modeled using two internal damage variables, d_2 (related to σ_{22}) and d_6 (related to σ_{12}). Based on CDM, the hypothesis of effective stress links the damage variables with the stresses, and Eq. (4) gives this relationship:

$$\begin{Bmatrix} \hat{\sigma}_{11} \\ \hat{\sigma}_{22} \\ \hat{\sigma}_{12} \end{Bmatrix} = \begin{bmatrix} 1/1-d_2 & 0 & 0 \\ 0 & 1/1-d_2 & 0 \\ 0 & 0 & 1/1-d_2 \end{bmatrix} \begin{Bmatrix} \sigma_{11} \\ \sigma_{22} \\ \sigma_{12} \end{Bmatrix} \tag{4}$$

where the $\hat{\sigma}_{ij}$ terms are the effective stress tensors.

According to Ribeiro et al. [6], the damage strain energy density can be described in function of effective stresses considering matrix phase stresses only, as shown in Eq. (5):

$$E_D = \frac{1}{2}\left[\frac{\langle\sigma_{22}^2\rangle_+}{E_{22_0}(1-d_2)} + \frac{\langle\sigma_{22}^2\rangle_-}{E_{22_0}} + \frac{|\sigma_{12}^2|}{G_{12_0(1-d_6)}}\right] \tag{5}$$

where $\langle\sigma_{22}^2\rangle_+ = \sigma_{22}^2$ if $\sigma_{22}^2 > 0$, otherwise $\langle\sigma_{22}^2\rangle_+ = 0$ if $\sigma_{22}^2 < 0$. Similarly, $\langle\sigma_{22}^2\rangle_- = -\sigma_{22}^2$ if $\sigma_{22}^2 < 0$, otherwise $\langle\sigma_{22}^2\rangle_- = 0$ if $\sigma_{22}^2 > 0$.

Ladeveze and LeDantec [21] introduced two thermodynamic forces into their model, which relates damage variables with the strain energy density (E_D), described in Eqs. (6) and (7):

$$Y_2 = \frac{\partial E_D}{\partial d_2} = \frac{\langle\sigma_{22}^2\rangle_+}{2E_{22_0}(1-d_2)^2} \tag{6}$$

$$Y_6 = \frac{\partial E_D}{\partial d_6} = \frac{\langle\sigma_{22}^2\rangle_+}{2G_{12_0}(1-d_6)^2} \tag{7}$$

Damage initiation in a composite can be identified as being the onset of damage due to stress reversals and the accumulation of inelastic strain (indication of appearance of a crack), which is assessed by carrying out cyclic quasi-static tests. The model regards that the damage process starts when the stress *vs.* strain curve is no longer linear.

Another characteristic of the present model is that it adjusts the Poisson's coefficient to take into account damage. Using CDM formulation performed by Matzenmiller et al. [22], Eq. (8) gives the stiffness tensor:

$$D = \frac{1}{K}\begin{bmatrix} (1-d_1)E_{11} & (1-d_1)(1-d_2)\nu_{21}E_{22} & 0 \\ (1-d_1)(1-d_2)\nu_{12}E_{11} & (1-d_2)E_{22} & 0 \\ 0 & 0 & K(1-d_6)G_{12} \end{bmatrix} \tag{8}$$

where $K = (1-(1-d_1)(1-d_2)\nu_{12}\nu_{21})$. To prevent material self-healing effect, the damage parameters (d_1, d_2 and d_6) are assumed the maximum calculated values along the simulation [6].

3. Computational models and experimental set-up

Computational models were developed on Abaqus™ 6.14 software platform (Fig. 1). The original dimensions of the tubes are: length (l) = 381 mm, inner radius (r) = 68 mm and lamina thickness (t_l) ≈ 0.6 mm. It is important to highlight that this thickness value is for ±φ winding plies. The composite structure was modeled by using S4R homogeneous reduced integration shell elements with three integration points per layer thickness and hourglass control (Fig. 1a). The rigid compressive plates were modeled as linear

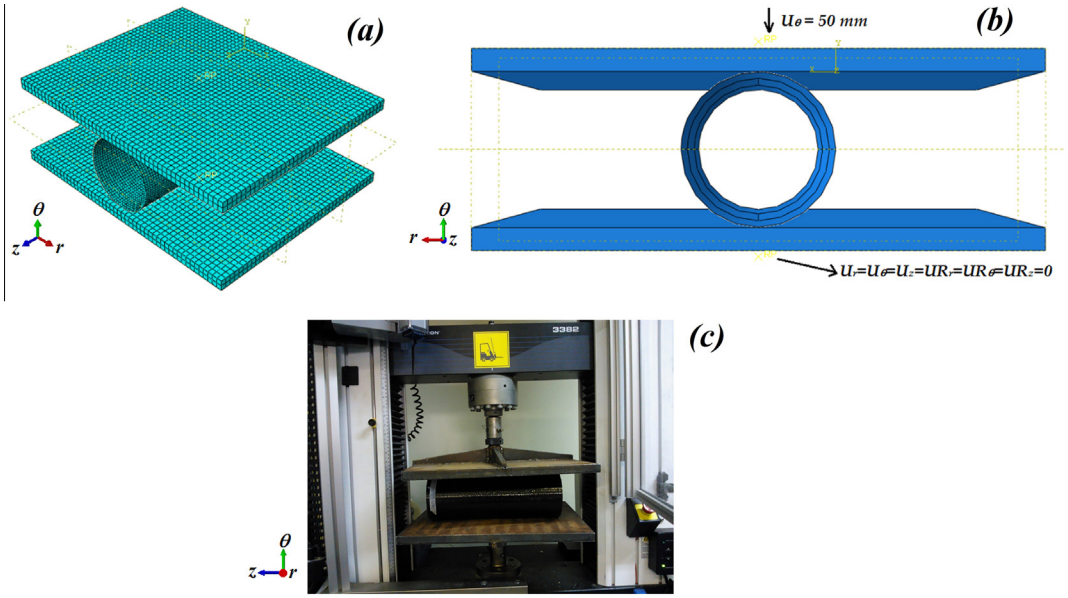

Fig. 1. Finite element mesh (a) and applied boundary conditions in the numerical model (b), and experimental set-up of the radial compression test (c).

quadrilateral elements of R3D4 type. The cylindrical shell was submitted to a radial compressive load by contact from the compression plates, which are simulated as rigid bodies, and where the boundary conditions (BC) were imposed (Fig. 1a–c).

Regarding the BCs, all displacements and rotations of the lower plate were restricted in all directions, whereas for the upper plate only the displacement in the θ-direction was released, where a maximum displacement of 50 mm was applied (Fig. 1b). The displacement of the upper plate was monitored and the reaction force of the upper reference point was collected. Compressive loading was transmitted to the tube by contact from the rigid compressive plates. A surface-to-surface contact algorithm was used to model plate-tube interaction by using small sliding formulation.

The proposed damage model was compiled as a UMAT (User Material Subroutine) and linked to the software used. The material properties of a representative unidirectional carbon/epoxy laminate with a fiber volume fraction of ≈70% (measured by acid digestion following ASTM D3171-15) has been used in the computational analyses [23] (Table 1). The damage model parameters were determined in standard tensile, compressive and shear tests, as well as in additional *off-axis* tests, which were reported in previous works [24–25].

Composite tubes were manufactured using towpregs from TCR Composites based on Toray T700-12K-50C carbon fiber and UF3369 epoxy resin system. A 1020 steel cylindrical mandrel with 381 mm length and 136 mm diameter was used to produce the tubes. The FW process was performed using a KUKA robot KR 140 L100 with MFTech's control and peripheral devices. After winding, a polyester-based shrink tape was used to wrap the laminate and aid compaction during curing, reducing voids. The system was then cured in an oven with air circulation at 130 °C for 4 h. After that, the system was cooled at room temperature, and the mandrel unscrewed to extract the composite tube.

Table 2 presents the different stacking sequences herein studied and their respective thicknesses. In order to facilitate identification of the laminate types, the indexes 1, 2 and 3 were used to refer to the amount of hoop layers. For all plies, the FW mosaic pattern was manufactured as being different, in order to increase resistance to crack propagation throughout the laminate thickness, as can be seen in Fig. 2. According to Morozov [26], if the position of fiber intercrossing in each particular ply does not overlap the previous and subsequent ones, the crack will find physical barriers to propagate itself.

Fig. 2 clarifies the pattern number (*PN*) for each ply within each laminate, which was chosen considering the degree of covering of each ply. Every pattern herein selected has a constant degree of covering of 100%.

The experimental test, according to ASTM D2412-11, concerns to the determination of the external load-deflection characteristics of a composite cylinder subjected to loading between two parallel steel bearing plates. The experiments have been performed in an Instron Universal machine model 3382 (Fig. 1c) under a crosshead speed of 12.5 mm/min. Five samples free of burrs and jagged edges of each stacking sequence family were tested, and the turnaround zones were cut off.

The tube stiffness (*TS*) and percentage tube deflection quota (P) parameters were obtained using Eqs. (9) and (10). Applying a

Table 1
Material properties used in the computational analyses.

	Symbol	Description	Value
Elastic constants	E_1 (GPa)	Longitudinal elastic modulus	129.3
	$E_2 = E_3$ (GPa)	Transversal elastic modulus	9.11
	$\nu_{12} = \nu_{21}$	Poisson's ratio in plane 1–2	0.32
	ν_{23}	Poisson's ratio in plane 2–3	0.35
	$G_{12} = G_{13}$ (GPa)	In-plane shear modulus	5.44
	G_{23} (GPa)	Transverse shear modulus in plane 2–3	2.10
Strengths	X_t (MPa)	Longitudinal tensile strength	1409.9
	X_c (MPa)	Transversal tensile strength	−740.0
	Y_t (MPa)	Longitudinal compressive strength	42.5
	Y_c (MPa)	Transversal compressive strength	−140.3
	S_{12} (MPa)	In-plane shear strength	68.9

Table 2
Nomenclature and characteristics of each laminate studied.

Nomenclature	Stacking sequence	Thickness (mm)
Type 1	[±45/±55/±89.6/±65/±75]	4.11
Type 2	[±89.6/±45/±55/±65/±89.6]	3.82
Type 3	[±89.6/±75/±89.6/±75/±89.6]	3.43

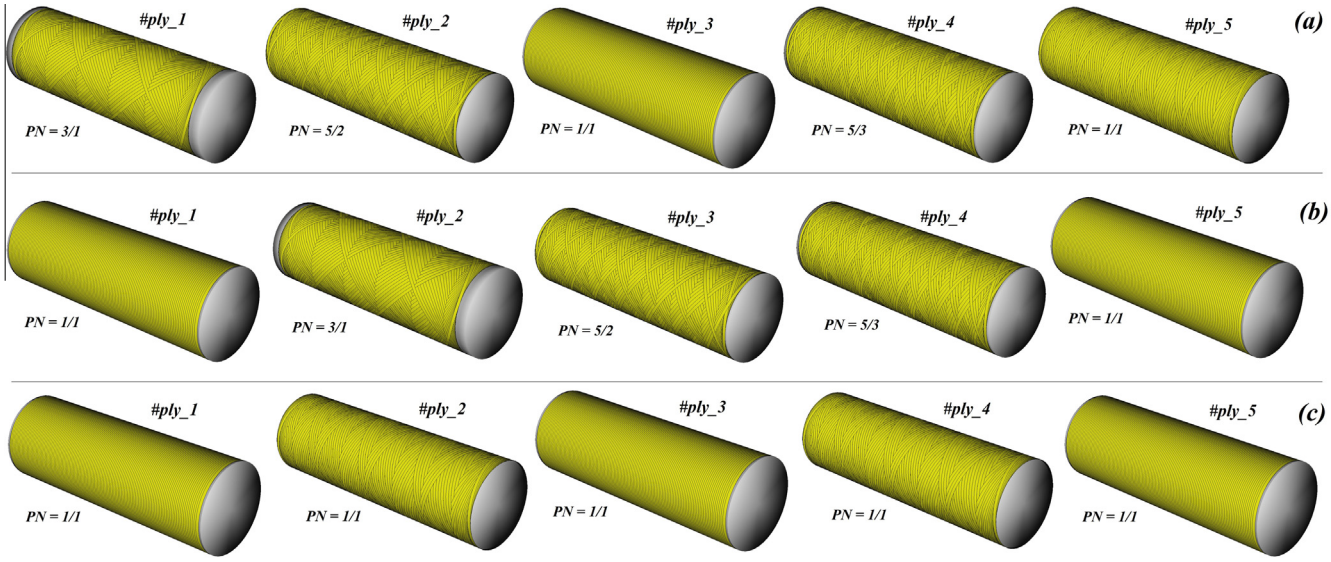

Fig. 2. Laminate configuration of each tube studied. The following laminates are presented: Type 1 – [±45/±55/±89.6/±65/±75] (a), Type 2 – [±89.6/±45/±55/±65/±89.6] (b) and Type 3 – [±89.6/±75/±89.6/±75/±89.6] (c).

correction factor ($C = (1 + \Delta_y/2d)^3$) to *TS*, it is assumed that the tube will kept elliptical during the load application.

$$TS = \frac{F}{\Delta_y}\left(1 + \frac{\Delta_y}{2d}\right)^3 \tag{9}$$

$$P = \frac{\Delta_y}{d} \times 100\% \tag{10}$$

where: F is the applied load, d is the outside diameter and Δ_y is the change in the outside diameter of the specimen in the load direction. The referred standard recommends that the change in inside diameter is reported, but as the samples had different wall thicknesses, the outside diameter was used to provide more comprehensive results, accounting for thickness on tube stiffness calculations. Eq. (11) was used to calculate the *SF*.

$$SF = EI = 0.149r^3 \times TS \tag{11}$$

where E is the elastic modulus, I is the moment of inertia of the tube, and r is the mid-wall radius, which is obtained by subtracting wall thickness from the outside diameter and dividing it by two.

4. Results and discussion

Fig. 3 presents the compressive load *vs.* deflection curves for the cylinders with different stacking sequences obtained using a linear-elastic model, in order to show the overall mechanical behavior of the structure. As can be noted, the compressive response of the tubes is highly dependent on ply orientation. Thus, as expected, this preliminary analysis indicates that plies wound at higher angles, i.e. closer to 90° (loading direction), improve the ability to withstand more load, as reported by Almeida Júnior et al. [27]. Moreover, ply homogenization [10] seems to have an effect on compressive response of cylinders, since the Type 1 and Type 2 laminates have similar winding angles, and although the first laminate has a hoop layer located at the middle ply, it supports less load than the second laminate, which does not have a hoop layer in the laminate. However, these assumptions must be deeper evaluated through progressive failure analysis.

Another preliminary study was carried out, which is the influence of model parameters on the global compressive response of the tubes. The model parameters analyzed are transverse shear stiffness (TSS) and non-linear geometric analysis (NLGEOM). Regarding the former, shell elements are based on first-order transverse shear flexible theory, in which the transverse shear strain is constant through the thickness of the laminate. This assumption demands the use of shear correction factors. The use of these factors also allows estimating interlaminar shear stresses in a composite section [28]. For this reason, TSS used in the FE models is defined by the user, as seen in Fig. 4. Regarding the effect of NLGEOM, it was assessed through Riks analysis [29] in order to predict whether buckling happens in the actual simulations [30].

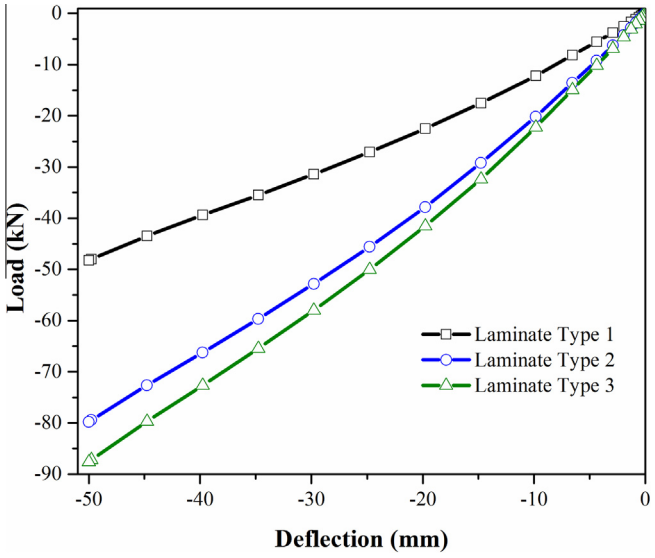

Fig. 3. Load *vs.* deflection curves predictions for linear-elastic models accounting for non-linear geometric effects.

The Type 1 laminate was chosen for this parametric analysis. TSS of a shell element is calculated at the beginning of a simulation and it is based on material stiffness and first-order shear deformations. As can be seen in Fig. 4, there is little difference between the curves for TSS calculated by the software and TSS inputted by the user. However, this difference increases towards the end of the simulation, and this may influence the numerical results.

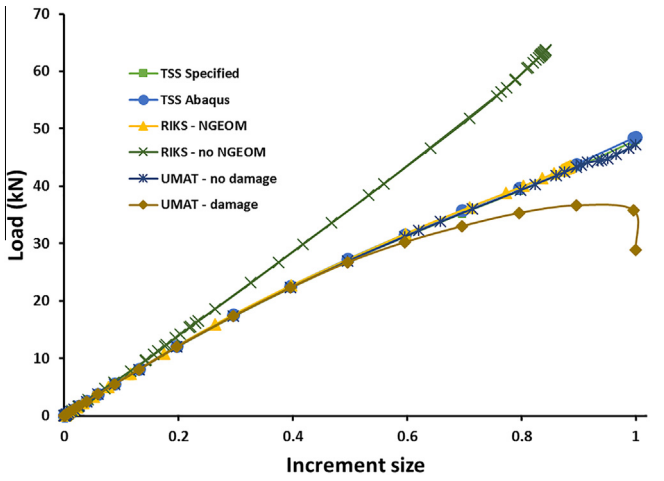

Fig. 4. Influence of model parameters on the radial compressive response for the Type 3 tube.

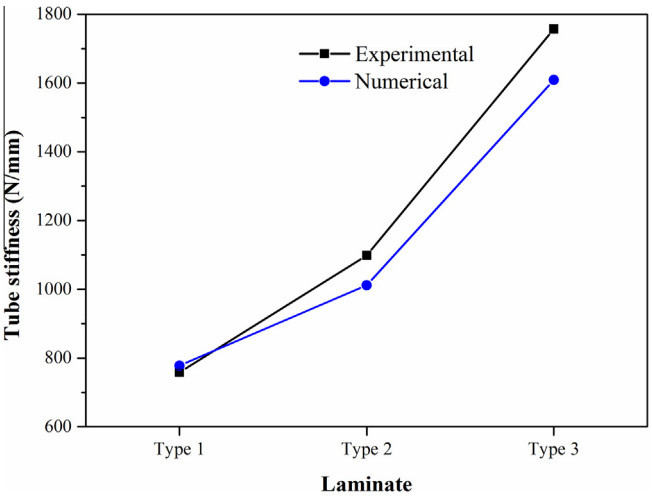

Fig. 6. Stiffness results of the studied tubes.

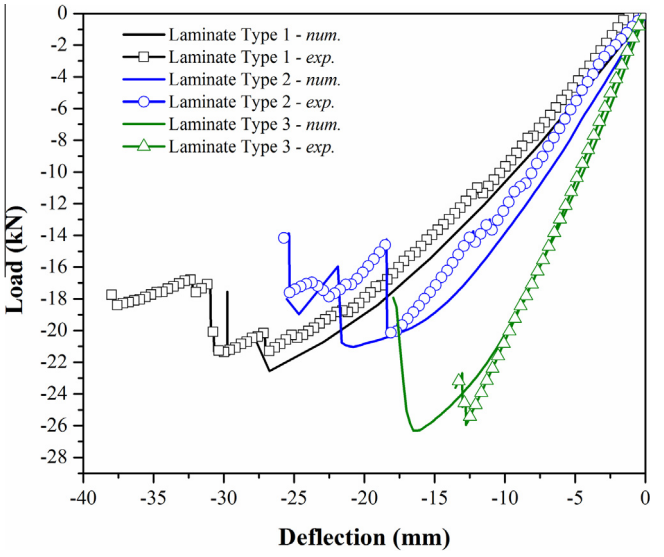

Fig. 5. Load *vs.* deflection for the tubes under radial compression: experimental and numerical results.

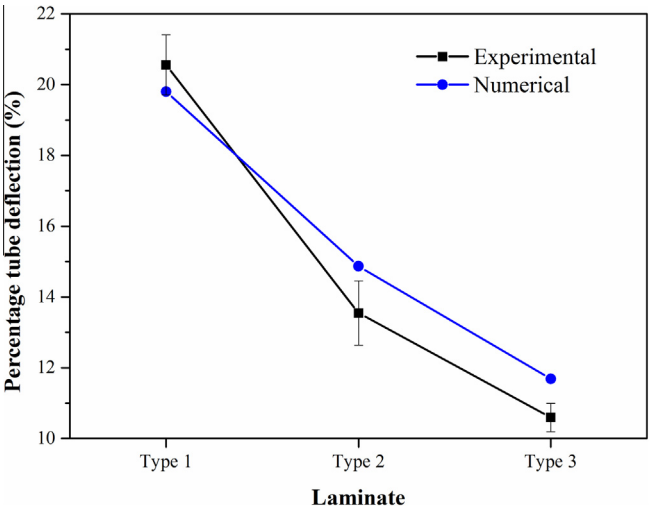

Fig.7. Percentage tube deflection for all tubes.

Concerning the analysis using Riks method, it is possible to predict buckling failure loads and mode. In order to ensure that buckling is not occurring in the current problem, a displacement of 500 mm is applied, and buckling is noticed only for a displacement of 209 mm, which is a high displacement considering the composite tubes studied. Thus, this is a strong evidence that the current analysis cannot be considered as an instability problem due to the high stiffness of the tubes. Simulations using the UMAT with and without damage have also been performed, where the native behavior of the linear-elastic analysis is recovered. Therefore, at high load and displacement levels, as found in Fig. 4, many plies fail, then catastrophic failure of the structure occurs.

Computational progressive failure analysis and experimental results of the composite tubes are presented in Fig. 5. The damage model simulates very well the behavior of the tubes [30]. That is, load *vs.* deflection curves, maximum load and stiffness of each stacking sequence family can be predicted with good accuracy.

Type 1 and Type 2 tubes show high non-linear behavior after −12 kN, which is related to delaminations. These failures take place after the maximum peak load as observed during experimental tests. On the other hand, the Type 3 tube show a quasi-brittle failure, as noticed in both experimental and numerical analyses, which occurs because it has all laminas wound very close to the circumferential direction, i.e. the loading direction. However, Type 1 and Type 2 laminates tubes support high deflection levels, which can be attributed to the pattern used, since the fiber intercrossing do not overlap in any lamina, hindering crack propagation.

The concept of tube stiffness can be used to compare numerical and experimental results, which are shown in Fig. 6. In general, experimental results and numerical predictions are very close for all laminate configurations, with a difference not higher than 6%. The tubes are highly dependent on the winding angle and winding mosaic pattern, and similar interpretations can be provided, since more layers wound closer to the load direction make the tube stiffer when loaded under radial compression. The opposite behavior is observed for tubes wound with ±45°, ±55° and ±65° layers, where the tubes are less stiff for this loading case.

The percentage tube deflection (Fig. 7) is associated with tube stiffness, and less stiff tubes tend to deflect more. In addition, although none of the tubes buckled, the absence of laminas wound at the loading direction allows higher deflection levels. As load in the tube increases, the cross-section changes from a perfect circle to an ellipse, i.e. dimensions in the vertical direction decreases

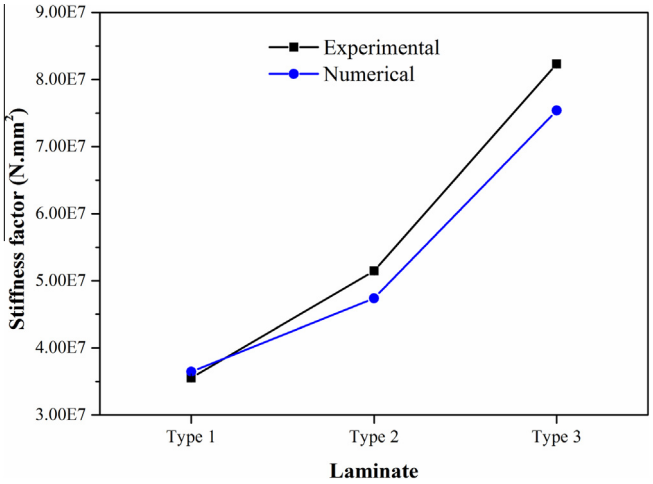

Fig. 8. Stiffness factor for all tubes.

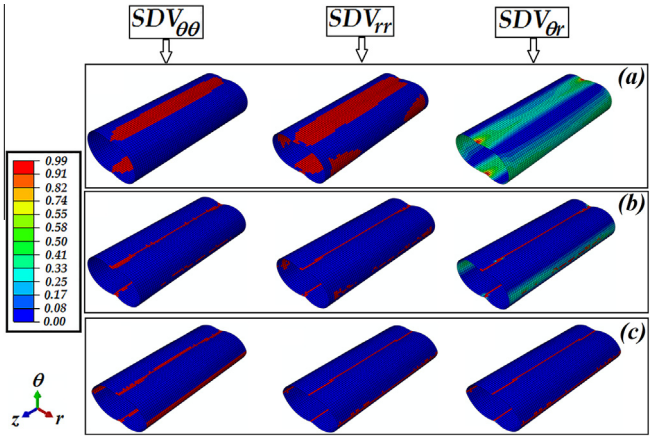

Fig. 9. Final deformed shape of the tubes highlighting the $SDV_{\theta\theta}$ (which is related to σ_{11}), SDV_{rr} (which is related to σ_{22}) and $SDV_{\theta r}$ (which is related to σ_{12}) for the filament wound tubes Type 1 a), Type 2 b) and Type 3 c).

and in the horizontal direction increases, being the later restricted by the lateral stiffness of the tube. The largest change typically occurs along the vertical and horizontal directions, being the vertical slightly larger than the horizontal.

Fig. 8 presents the stiffness factor (SF) for all tubes, which is a useful parameter since it indirectly correlates the flexural modulus and the wall thickness ($I = \frac{t^3}{12}$). As SF is highly dependent on tube deflection, the results corroborate those of the deflection (Fig. 8).

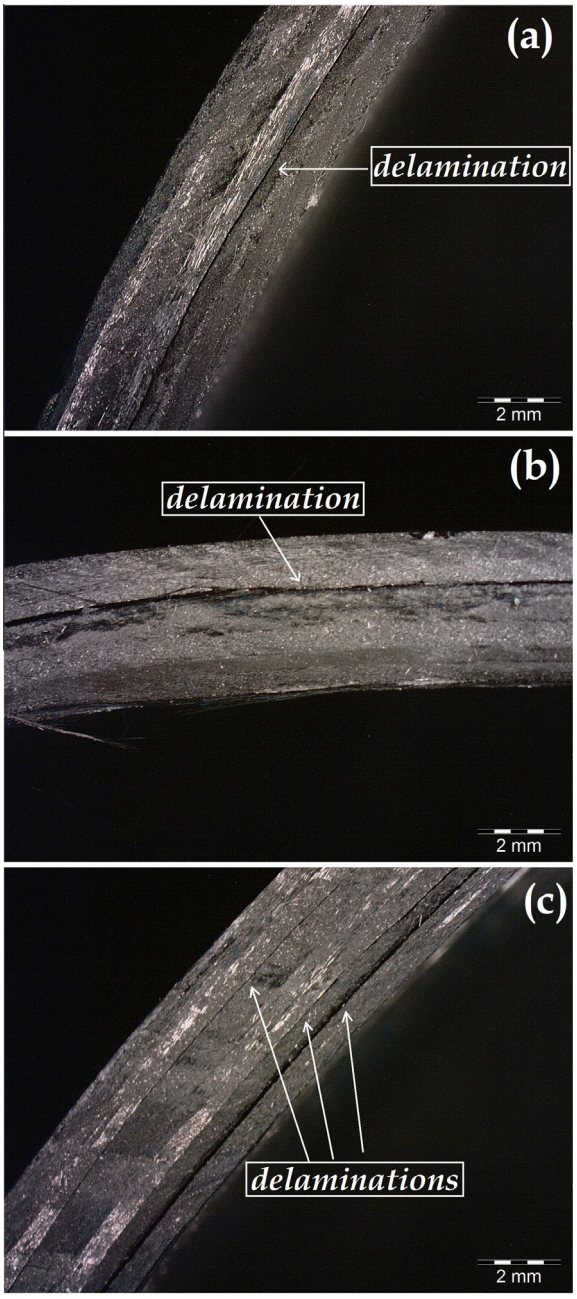

Fig. 11. Stereoscopic analysis of the tubes Types 1 (a), 2 (b), and 3 (c).

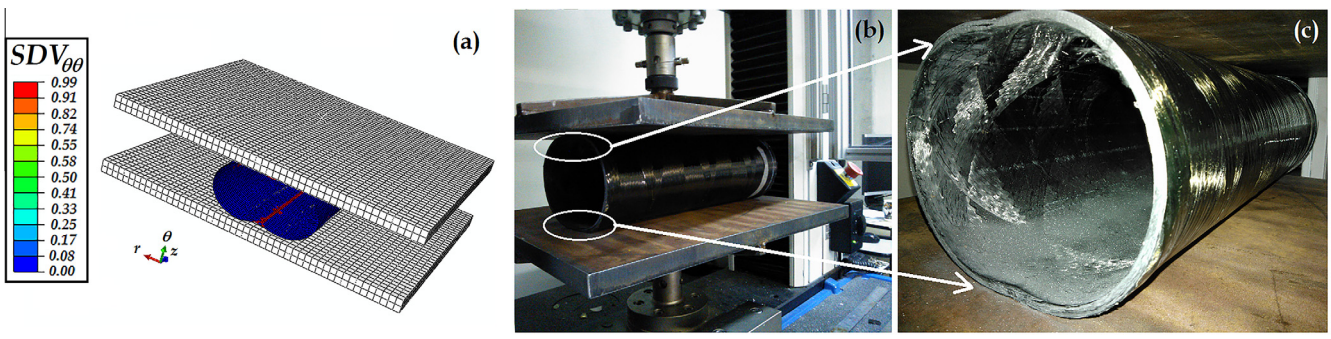

Fig. 10. Damage in fiber direction at the final failure (a), and view of the type 1 tube just prior to failure highlighting delaminations (b and c).

In other words, the specimen with more layers in the circumferential direction has higher SF.

Fig. 9 shows the deformed shape of all studied tubes concerning their damage in the fiber axial direction ($SDV_{\theta\theta}$), related to normal stresses ($\sigma_{\theta\theta}$), in the fiber radial direction (SDV_{rr}), related to transverse stresses (σ_{rr}), and shear stresses in plane θ–r ($SDV_{\theta r}$), related to in-plane shear stresses ($\sigma_{\theta r}$). It is clear that all tubes deform elliptically. Also, the tubes present stress concentrations at the contact areas with the compressive plates and transversally to them. Most tubes show more damaged regions at the contact area with the compressive plates. It is valid to mention that the finite element mesh was sufficient refined, based on a balance efficiency between accurate results and simulation time, but also avoiding edge effects caused by plate-tube-plate contact, which was observed in less refined meshes. All tubes presented high shear stress levels at the final failure. In addition, large shear stress levels have been detected in the vertical edges of the composite tube, which may strongly induce failure by delaminations. Furthermore, the deformed shapes of the damaged tubes demonstrate that buckling does not happen for the investigated stacking sequences.

Fig. 10 presents the final shape of the actual Type 1 tube and it can be seen that delamination is the main failure mode. Even with many delaminations at large deflections, the composite tube keeps carrying load and retaining some structural integrity, aiding interpretation of numerical and experimental results presented in Fig. 5. Fig. 10a–c) confirm that the composite tubes under radial compression present delaminations, which generate circumferential cracks near the specimen mid-thickness.

In order to identify more accurately the failure modes, stereoscopic images are presented in Fig. 11. As previously discussed, delaminations drive the failure mode of the investigated tubes under radial compression loading. These images can help explaining why Type 3 tube shows better structural response than the others. The other tubes have one main delamination that lead to catastrophic failure, followed by many smaller cracks caused by the progressive failure of the laminas. For Type 3 specimens, multiple delaminations are found, which is related to the winding of more layers in the loading direction.

5. Conclusions

The focus of this study was the development of a computational model with damage to simulate the radial compressive behavior of filament wound composite tubes with different stacking sequences. The tubes started concentrating stress at the outermost layers due to their contact with the device loading plates and damage propagated from the contact areas. As expected, the tubes reduced in diameter in the vertical direction, and expanded in the horizontal direction, generating an elliptical deformed shape. The computational model has accurately predicted both load and deflection as compared to the experimental results.

The stacking sequence strongly affected maximum load supported by the composite tubes, and the tube with more hoop layers as the outer layers of the laminate and with non-geodesic layers wound at ±75° showed better structural response. Different winding patterns for the laminas in the same laminate influenced compressive strength due to fiber inter-crossing at different positions.

Finally, delaminations were the main failure mode for all investigated tubes, showing that wound composite tubes designed to withstand radial compressive loading need to be manufactured with hoop layers as inner and outer layers, along with ±75° non-geodesic layers. This type of stacking sequence yields maximum compressive load, since the reinforcement is wound closer to the loading direction.

Acknowledgments

The authors are grateful to CAPES, CNPq and AEB (Brazilian Space Agency) for the financial support. Marcelo Ribeiro and Volnei Tita would like to thank FAPESP (2015/13844-8) and CNPq (401170/2014-4 and 310094/2015-1).

References

[1] Rafiee R. On the mechanical performance of glass-fibre-reinforced thermosetting-resin pipes: a review. Compos Struct 2016;143:151–64.
[2] Ribeiro ML, Vandepitte D, Tita V. Experimental analysis of transverse impact loading on composite cylinders. Compos Struct 2016;133:547–63.
[3] Almeida Júnior JHS, Faria H, Marques AT, Amico SC. Load sharing ability of the liner in type III composite pressure vessels under internal pressure. J Reinf Plast Compos 2014;33(24):2274–86.
[4] Singer J, Arbocz J, Weller T. Buckling experiments: experimental methods in buckling of thin-walled structures. Shells, built-up structures, composites and additional topics, vol. 2. New York: John Wiley & Sons, Inc; 2002.
[5] Tafreshi A. Delamination buckling and postbuckling in composite cylindrical shells under combined axial compression and external pressure. Compos Struct 2006;72(4):401–18.
[6] Mistry J, Gibson AG, Wu Y-S. Failure of composite cylinders under combined external pressure and axial loading. Compos Struct 1992;22(4):193–200.
[7] Camanho PP, Miamí P, Dávila CG. Prediction of size effects in notched laminates using continuum damage mechanics. Compos Sci Technol 2007;67(13):2715–27.
[8] Su ZC, Tay TE, Ridha M, Chen BY. Progressive damage modeling of open-hole composite laminates under compression. Compos Struct 2015;122:507–17.
[9] Liu PF, Zheng JY. Progressive failure analysis of carbon fiber/epoxy composite laminates using continuum damage mechanics. Mater Sci Eng A 2008;485:711–7.
[10] Melo JDD. LamRank, a laminate design tool. JEC Compos Mag 2014;88:49–51.
[11] Silvestre N. Buckling behaviour of elliptical cylindrical shells and tubes under compression. Int J Solids Struct 2008;45:4427–47.
[12] Jia X, Chen G, Yu Y, et al. Effect of geometric factor, winding angle and pre-crack angle on quasi-static crushing behavior of filament wound CFRP cylinder. Compos B 2012;45(1):1336–46.
[13] McGregor CM, Vaziri R, Poursartip A, Xiao X. Simulation of progressive damage development in braided composite tubes under axial compression. Compos A 2007;38(11):2247–59.
[14] Faria H, Guedes RM. Long-term behaviour of GFRP pipes: reducing the prediction test duration. Polym Test 2010;29(3):337–45.
[15] Guedes RM, Sá A, Faria H. On the prediction of long-term creep-failure of GRP pipes in aqueous environment. Polym Compos 2010;31(6):1047–55.
[16] Rafiee R. Experimental and theoretical investigations on the failure of filament wound GRP pipes. Compos B 2013;45:257–67.
[17] Tonatto MLP, Forte MMC, Tita V, Amico SC. Progressive damage modeling of spiral and ring composite structures for offloading hoses. Mater Des 2016;108:374–82.
[18] Ribeiro ML, Tita V, Vandepitte D. A new damage model for composite laminates. Compos Struct 2012;94(2):635–42.
[19] Herakovich C. Mechanics of fibrous composites, vol. 1. Wiley Publisher; 1998.
[20] Puck A, Schürmann H. Failure analysis of FRP laminates by means of physically based phenomenological models. Compos Sci Technol 1998;58(7):1045–67.
[21] Ladeveze P, LeDantec E. Damage modelling of the elementary ply for laminated composites. Compos Sci Technol 1992;43(3):257–67.
[22] Matzenmiller A, Lubliner J, Taylor RL. A constitutive model for anisotropic damage in fiber-composites. Mech Mater 1995;20(2):125–52.
[23] Almeida Junior JHS, Souza SDB, Botelho EC, Amico SC. Carbon fiber-reinforced epoxy filament-wound composite laminates exposed to hygrothermal conditioning. J Mater Sci 2016;51(9):4697–708.
[24] Ribeiro ML, Vandepitte D, Tita V. Damage model and progressive failure analyses for filament wound composite laminates. Appl Compos Mater 2013;20(5):975–92.
[25] Tita V, Carvalho J, Vandepitte D. Failure analysis of low velocity impact on thin composite laminates: experimental and numerical approaches. Compos Struct 2008;83(4):413–28.
[26] Morozov EV. The effect of filament-winding mosaic patterns on the strength of thin-walled composite shells. Compos Struct 2006;76(1–2):123–9.
[27] Almeida Jr JHS, Ribeiro ML, Tita V, Amico SC. Buckling and post-buckling in filament wound composite tubes under transverse compression. In: Proceedings of the 20th international conference on composite materials; July 19–24; Copenhagen, Denmark. MCI Scandinavia. p. 1–10.
[28] Abaqus User's Manual. Abaqus Version 6.14 Documentation, Dassault Systèmes SIMULIA; 2014.
[29] Riks E. An incremental approach to the solution of snapping and buckling problems. Int J Solids Struct 1979;15(7):529–51.
[30] Almeida Jr JHS, Ribeiro ML, Tita V, Amico SC. Damage and failure in carbon/epoxy filament wound composite tubes under external pressure: Experimental and numerical approaches. Mater Des 2016;96:431–8.